

Article

Arrhenius Equation-Based Cell-Health Assessment: Application to Thermal Energy Management Design of a HEV NiMH Battery Pack

Yalian Yang¹, Xiaosong Hu^{2,3,*}, Datong Qing¹ and Fangyuan Chen¹

¹ State Key Laboratory of Mechanical Transmission (SKLMT), Chongqing University, Chongqing 400030, China; E-Mails: yyl@cqu.edu.cn (Y.Y); dtqin@cqu.edu.cn (D.Q); chenfangyuan001@yahoo.com.cn (F.C)

² National Engineering Laboratory for Electric Vehicles, Beijing Institute of Technology, Beijing 100081, China

³ Department of Signals and Systems, Chalmers University of Technology, 41296 Gothenburg, Sweden

* Author to whom correspondence should be addressed; E-Mails: xiaosong@chalmers.se or huxstank@bit.edu.cn; Tel.: +46-31-772-1538; Fax: +46-31-772-1748.

Received: 22 January 2013; in revised form: 15 May 2013 / Accepted: 16 May 2013 /

Published: 22 May 2013

Abstract: This paper presents a model-based cell-health-conscious thermal energy management method. An Arrhenius equation-based mathematical model is firstly identified to quantify the effect of temperature on the cell lifetime of a Nickel Metal Hydride (NiMH) battery pack. The cell aging datasets collected under multiple ambient temperatures are applied to extract the Arrhenius equation parameters. The model is then used as an assessment criterion and guidance for the thermal management design of battery packs. The feasibility and applicability of a pack structure with its cooling system, is then evaluated, and its design problems are studied by a computational fluid dynamics (CFD) analysis. The performance and eligibility of the design method is validated by both CFD simulations and experiments.

Keywords: battery thermal management; battery health; electrified vehicle

1. Introduction

Energy supply uncertainty, volatile oil prices, and increasingly stringent regulations on pollutants and carbon footprint pose heavy challenges for today's fossil fuel-dominant ground transportation [1,2]. To accelerate the shift to sustainable transportation, electrified vehicles, such as battery electric vehicles (BEVs), hybrid electric vehicles (HEVs), and plug-in hybrid electric vehicles (PHEVs), are being studied and developed around the globe [3–5]. The traction battery packs have a significant impact on the performance, cost, and reliability of electrified vehicles. An efficient battery management system (BMS) is thus required to ensure safe and reliable battery operations in complex and highly dynamic onboard environment [6–9].

A key task of BMS is to manage cell temperature to avoid overheating and to reduce large temperature gradients among cells. Temperature has been recognized as the dominant stressing factor for battery degradation [10]. Both high temperature and large temperature gradients lead to reduced cell life. Diverse methods of battery thermal management were studied. For example, phase change materials which can absorb large amounts of heat were often used to control thermal runaways under extreme conditions [11–14]. Active methods, e.g., liquid-cooled and air-cooled systems, were also adopted [15,16]. A comparison of the effectiveness of the two types of methods was investigated in [17]. Heat pipes were also used to cool the battery system [18]. Several commonly used battery cooling techniques are compared in [19]. The vast majority of relevant literature was focused on the thermal behavior of the cooling material, and the performance of different approaches in preventing unsafe temperatures is compared. Studies on the cell temperature uniformity, however, are relatively scarce. A rule-of-thumb threshold, e.g., 5 °C, was often used as limit to the temperature nonuniformity for batteries of different chemistries, or from different manufacturers. Little research has been done to study how small the temperature gradient should be for a specific battery to ensure cell health. Since different batteries typically have considerably different aging characteristics, the same temperature deviation will induce different degradations for different batteries. A mathematical model that can explicitly capture the relationship between cell temperature and degradation would be beneficial to addressing this problem. According to the requirement for the cell health uniformity, the model can be used to assessing the acceptable level of temperature gradient, thus predicting degradation and guiding cooling system design. The main contributions of this paper are the development of such a model and its application to temperature-gradient management for cells inside a battery pack.

In this paper, the effect of temperature deviation on cell degradation consistency is modeled using the Arrhenius equation, based on experimental data collected on Nickel Metal Hydride (NiMH) cells. According to the calibrated model and cell health-consistency requirement, the feasibility and applicability of a NiMH battery pack design, together with its air cooling system, is experimentally evaluated for an HEV prototype manufactured by Changan Automobile Company Limited in Chongqing city in China. The shortcomings of the current design are analyzed using computational fluid dynamics (CFD). Subsequently, an improved design is proposed. The performance of the new design is validated by means of CFD simulations and experimental analysis.

The remainder of this paper is organized as follows: in Section 2, the mathematical model describing the influence of the temperature discrepancy on the lifetime consistence of NiMH cells is presented. Based on the model, Section 3 presents the assessment of a NiMH battery pack design,

along with its cooling system. The design deficiencies are also analyzed. An improved design solution is depicted in Section 4, in which simulation and experimental analysis are applied to demonstrate its performance. Finally, conclusions are drawn in Section 5.

2. Effect of Temperature Gradient on Cell Degradation Variation

Cell temperature has a large impact on cell health degradation: the higher the temperature, the faster the rate of aging [20]. Therefore, non-uniform temperatures will result in different cell health levels within the same pack. The cell with the highest degradation usually determines the lifetime of the whole pack. To facilitate effective thermal management system design, it is important to build a mathematical model that can accurately quantify the effect of temperature gradients on cell lifetime uniformity.

2.1. Model Structure Based on Arrhenius Equation

The Arrhenius equation is a succinct, but precise characterization of the temperature dependence of the rate of a chemical reaction [21]. It was often applied to model the temperature-induced alteration of diffusion coefficients, creep rates, and other thermal processes [22]. The Arrhenius equation was also used to delineate the temperature-dependent degradation rates of electrochemical cells [23–25]. The basic Arrhenius equation is shown as follows:

$$\frac{dC}{dn} = \Lambda e^{-\frac{\Delta E}{RT}} = \Lambda e^{-\frac{\lambda}{T}} \quad (1)$$

where dC/dn is the rate of cell capacity change with respect to aging cycle, Λ is the pre-exponential factor, and R is the universal gas constant [*i.e.*, 8.314 J/(mol K)]. ΔE and T are activation energy in the unit of J/mol and absolute temperature in the unit of K, respectively [21,22]. Here, we view Equation (1) as an empirical formula such that Λ and $\lambda = \Delta E/R$ are interpreted as two unknown parameters to be calibrated. Integrating both sides of Equation (1) over the cell lifespan yields:

$$C_r = -\Lambda n_c e^{-\frac{\lambda}{T}} \quad (2)$$

where C_r is the capacity reduction threshold indicative of the cell failure, and n_c is the cycle life. Assign two different temperatures, T_1 and T_2 ($T_1 > T_2$), to Equation (2) to constitute:

$$\Delta n_c = \frac{C_r}{\Lambda} \left(e^{\frac{\lambda}{T_2}} - e^{\frac{\lambda}{T_1}} \right) \quad (3)$$

where Δn_c is the lifetime deviation. It is evident that Equation (3) is a quantitative description of the effect of the temperature gradient on cell life.

2.2. Model Parameter Calibration

2.2.1. Linear Identifiable Form

An identifiable form of the model is obtained by taking the natural logarithm of both sides of Equation (2):

$$\ln\left(\frac{C_r}{n_c}\right) = \ln(-\Lambda) - \frac{\lambda}{T} = \underbrace{\left[1 \quad -\frac{1}{T}\right]}_{\boldsymbol{\varphi}} \underbrace{\begin{bmatrix} \ln(-\Lambda) \\ \lambda \end{bmatrix}}_{\boldsymbol{\theta}} \quad (4)$$

where $\boldsymbol{\varphi}$ is the regressor, and $\boldsymbol{\theta}$ is the parameters to be identified. For electrified vehicle applications, C_r is often specified as 20%. In order to extract the unknown parameters, the cell cycle life n_c under different temperatures should be determined or estimated.

2.2.2. HEV NiMH Cell Aging Test

NiMH cells from the same batch for an HEV prototype manufactured by Changan Company were tested. The testing system can implement diverse charging/discharging modes, monitor and record cell current, voltage, and power, as well as implement safety protection. The nominal capacity and voltage of the NiMH cells are 6.5 Ah and 1.2 V. The upper and lower cut-off voltages are 1.55 V and 1.05 V, respectively. The aging cycle was chosen to be constant-current full charge and discharge at the rate of 1 C, and the cell static capacity was calibrated every 10 cycles to record the cell degradation levels. Three aging tests were conducted under 25 °C, 40 °C, and 50 °C, respectively. In each test, five NiMH cells were cycled, and then the average capacity was calculated and used to take the cell manufacturing variance into account. Simple aging cycles are used because our goal is to identify the relationship between the cell health and operating temperature, as opposed to establishing a complete battery degradation model as a function of temperature, current rate, and depth of discharge (DOD). Furthermore, since in practice the cells in the pack undergo approximately the same current and DOD, the cell health inconsistency is mainly attributed to the cell temperature deviation. The measured capacities under the three aging tests are shown in Figure 1. The capacity reduction is shown in Figure 2.

Figure 1. Cell capacities under three different temperatures.

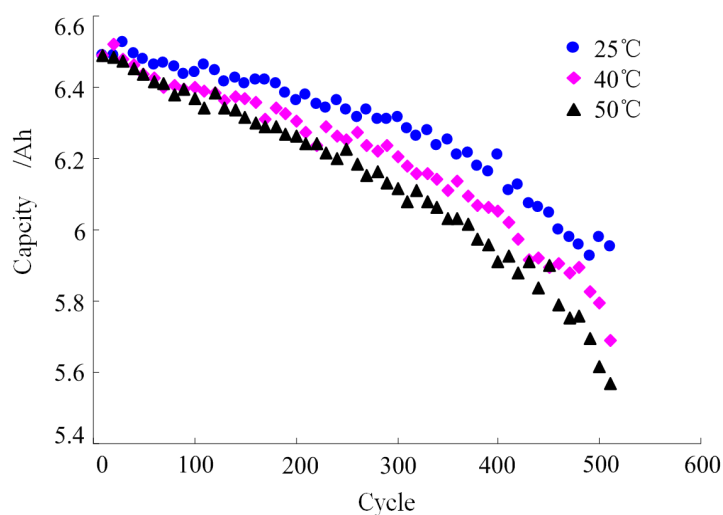
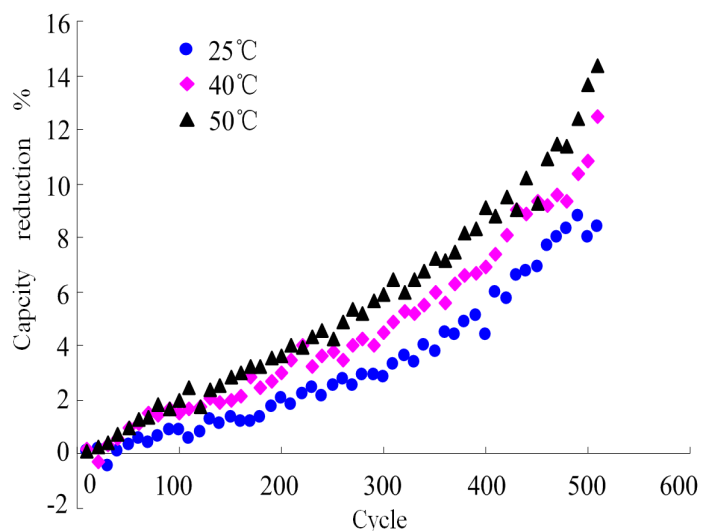


Figure 2. Capacity percent reductions.



It is clear that the cell degraded most rapidly under 50 °C. Notice that since the aging tests did not damage the cells up to failure, this necessitates estimating the cell life based on the available capacity history. From Figure 2, it can be observed that the trajectory of the capacity reduction is a quadratic-function of the number of aging cycles. We use a nonlinear least-squares optimization algorithm to identify the parameters of the quadratic function. The results for the three temperatures are shown in Table 1. For $C_d = C_r = 20\%$, the solutions are shown in Table 2.

Table 1. Quadratic functions depicting the relationship between capacity reduction and the number of aging cycles.

Temperature/°C	Quadratic function/%
25	$C_d = 3.2 \times 10^{-5} n^2 - 9.8 \times 10^{-4} n + 0.21$
40	$C_d = 2.6 \times 10^{-5} n^2 + 6 \times 10^{-3} n + 0.15$
50	$C_d = 2.3 \times 10^{-5} n^2 + 9 \times 10^{-3} n + 0.13$

Table 2. Estimated cell cycle lifetime at the three temperatures.

Temperature/°C	25	40	50
Cycle life	801.87	765.96	754.19

2.2.3. Least-Squares Algorithm Based Parameterization

The least-squares algorithm is used to estimate the optimal model parameters using the following equation:

$$\hat{\theta} = (X^T X)^{-1} X^T y \tag{5}$$

where

$$X^T = [\varphi(T_1)^T \quad \varphi(T_2)^T \quad \varphi(T_3)^T] \tag{6}$$

$$y = \left[\ln\left(\frac{C_r}{n_{c,T_1}}\right) \quad \ln\left(\frac{C_r}{n_{c,T_2}}\right) \quad \ln\left(\frac{C_r}{n_{c,T_3}}\right) \right]^T \quad (7)$$

T_1 , T_2 and T_3 are the three operating temperatures. After obtaining $\hat{\theta}$, we can determine the model parameters:

$$\Lambda = -e^{\hat{\theta}(1)} \quad (8)$$

$$\lambda = \hat{\theta}(2) \quad (9)$$

The identification result is shown in Table 3, and the mean square error of the fitting is 4.04×10^{-5} . Note that thanks to the nonlinear Equation (8), the standard error of Λ is derived from Monte Carlo simulation, based on statistics (mean and standard deviation) of $\hat{\theta}(1)$. It is clear from error analysis that the fitting equation has good accuracy.

Table 3. Optimal model parameters and error bounds identified by the least squares method.

Result	Λ	λ
Estimate	-5.61×10^{-4}	240.74
Standard error (1 Sigma)	6.20×10^{-5}	34.29

2.3. Assessment Criterion

HEVs are often subject to complicated traffic and climate conditions so that the on-board battery packs undergo varying loads and ambient temperatures. Because the cells suffer more severe degradation at high temperatures, leading to shorter life, the temperature deviation among cells in a hot vehicle environment is of great concern. A performance index proposed by the HEV manufacturer requires that the cell life inconsistency for the battery cells should be less than 1.5% when the temperature is higher than 35 °C [26]. According to Equation (3), the maximum allowable temperature gradient among cells can be efficiently calculated to be 6 °C, which will serve as a performance assessment criterion and a design guide for the subsequent thermal energy management system of the HEV NiMH battery pack.

3. Feasibility Assessment of Primitive NiMH Battery Pack Design with its Cooling System

3.1. Experimental Analysis

The configuration of a prototype NiMH battery pack with no consideration of the impact of temperature discrepancy on cell health consistency is shown in Figure 3. It consists of three layers. The first layer contains 36 cells arranged in 3 rows and 12 columns, and there are 42 cells in the form of 3 rows and 14 columns for each of the other two layers. Notice that all 120 cells are electrically connected in series to increase the voltage level, as the HEV with an integrated starter/generator propulsion system has a low degree of hybridization which does not require a lot of energy. The cell dimensions and main electrical specifications are listed in Table 4. Five air ducts are designed for each

cell, as shown in Figure 3. The cells in each layer were cooled by two fans placed symmetrically. T-shaped thermocouples were used to collect the cell temperature data. The measurement points were selected considering the structural characteristics of each layer. There are 12 sensors in the first layer shown in Figure 4, and the remaining layers each have 15 sensors shown in Figure 5.

Figure 3. Configuration of the primitive HEV NiMH battery pack: 36 cells (3 rows and 12 columns) in the first (top) layer; 42 cells (3 rows and 14 columns) in each of the other layers.

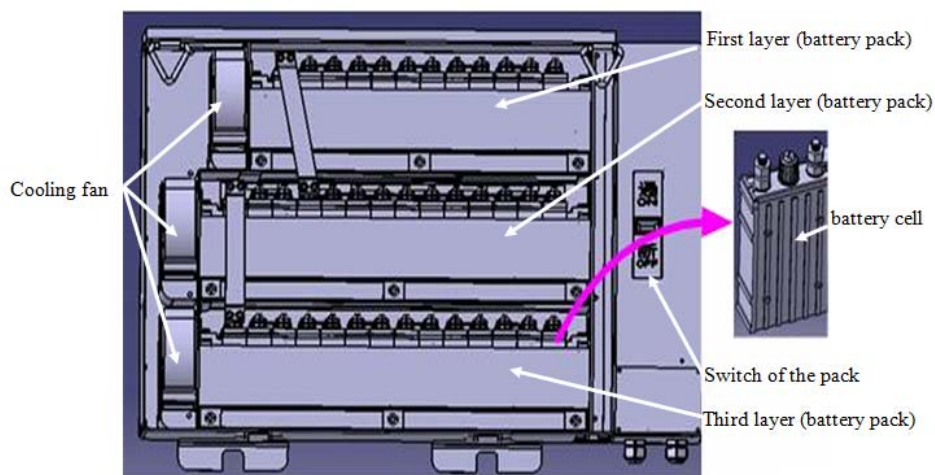


Table 4. Cell dimensions and main electrical specifications.

Thickness	23.5 mm
Width	60 mm
Height	84 mm
Weight	180 g
Nominal Voltage	1.2 V
Nominal Capacity	6.5 Ah
Power Density	≥ 1400 W/kg
Energy Density	≥ 44 Wh/kg
Ambient Temperature	-40 ~ 80 °C
Working Temperature	-30 ~ 60 °C
Usable SOC range	30% ~ 80%

Figure 4. Sensor location in the first layer.

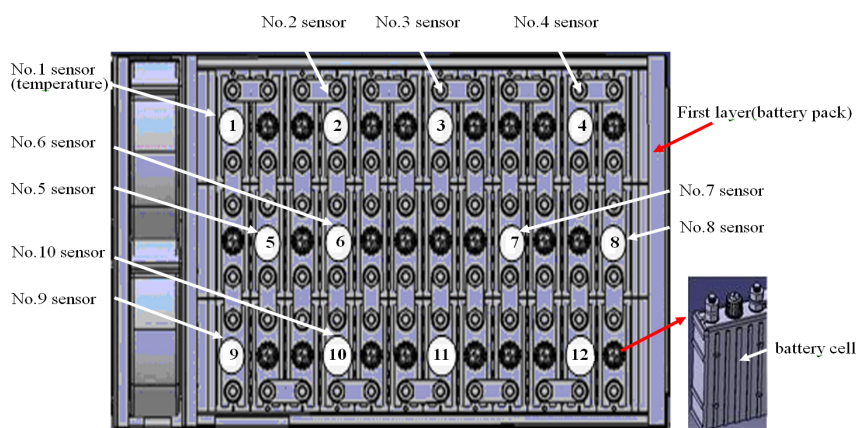
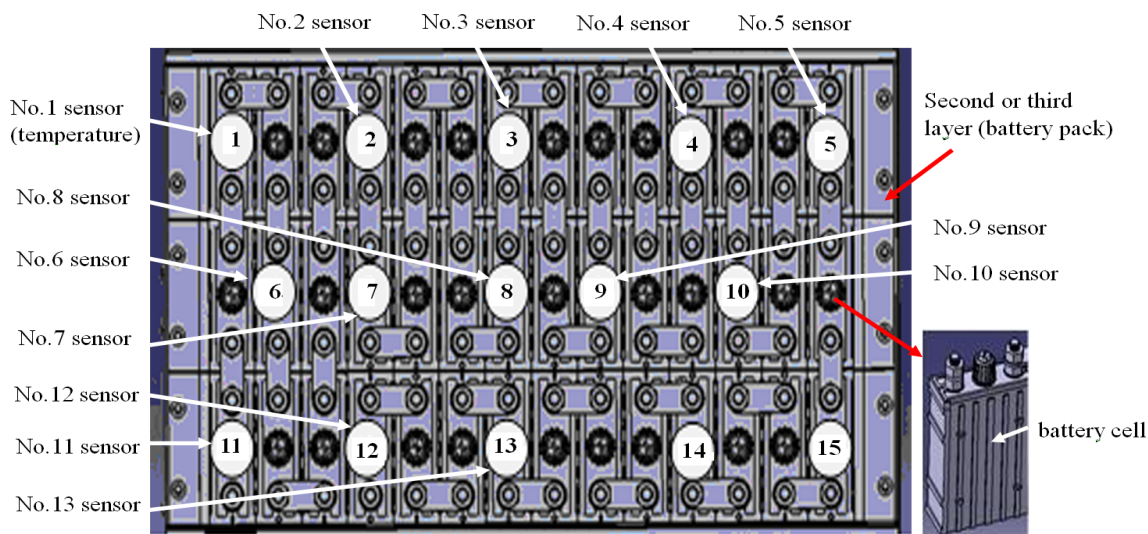


Figure 5. Sensor location in the second and third layers.



The road testing of the HEV vehicle with the prototype battery pack was conducted in a test field by DongFeng Motor Company Limited in Xiangfan city, China, during a hot summer. The test involved diverse road conditions and driving patterns. Please refer to [27] for more details on the test procedures. We measured the cell temperature in a 4.5 minute idling process intentionally designed as part of the test. The measured temperatures are shown in Figures 6–8. It can be seen that the cell with the highest temperature of 45.5 °C occurred in the third layer of the pack, while the lowest one with 36 °C is in the second layer. The maximum temperature difference is thus 9.5 °C. Taking a closer examination, we can find that the largest temperature discrepancy in the first layer is around 5.1 °C, and those for the second and third layers are 8 °C and 7.5 °C. It is clear that the preliminary battery pack and its cooling system design cannot meet the performance requirement of a maximum temperature difference of 6 °C.

Figure 6. Temperature measurement in the first layer.

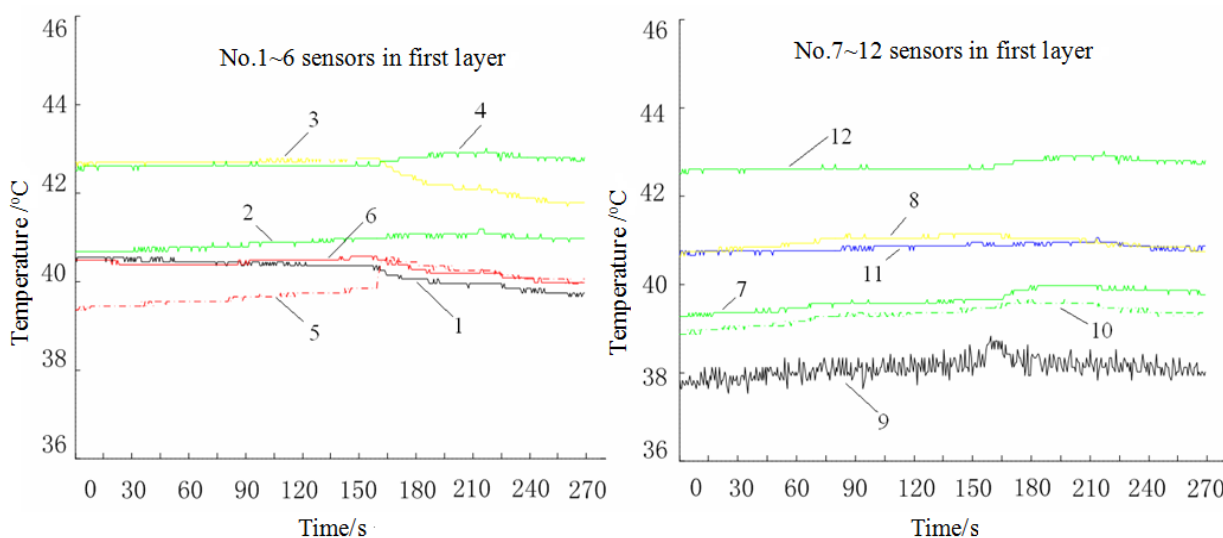
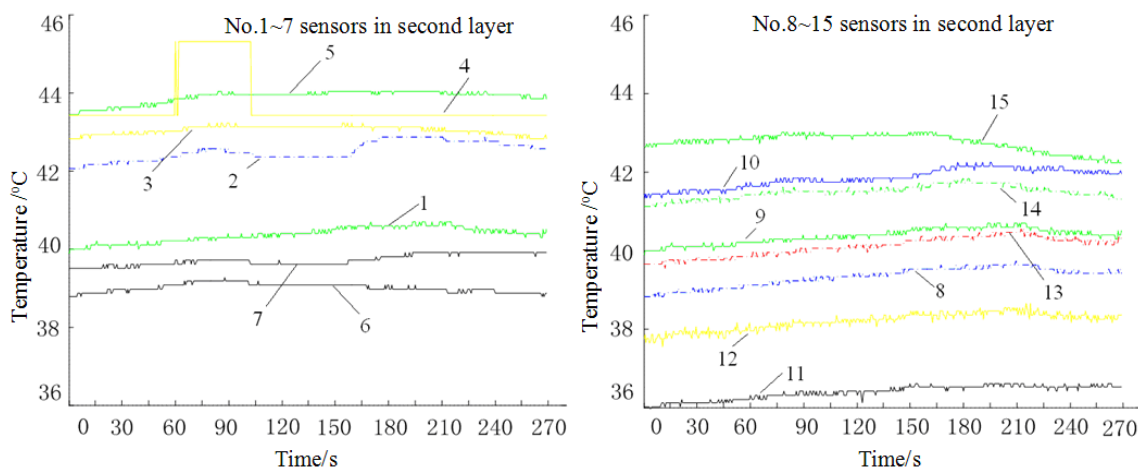
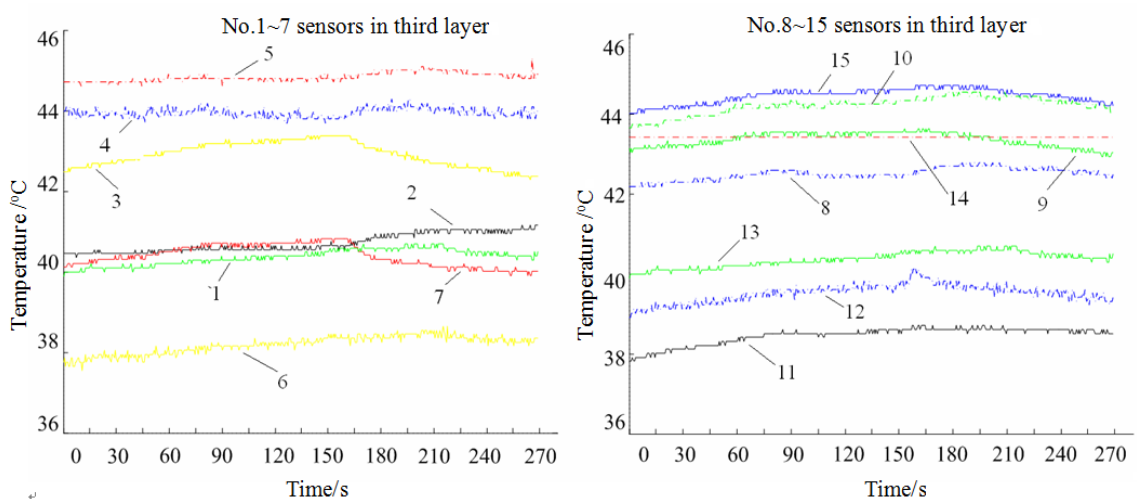


Figure 7. Temperature measurement in the second layer.**Figure 8.** Temperature measurement in the third layer.

3.2. Analysis of the Shortcomings of the Preliminary Design

Since the pack structure is quite complicated, a flow field analysis was performed first to investigate the air flow allocation among the three layers. The CFD model of the pack is shown in Figure 9. The air inlet and outlet were designated as the pressure import and the pressure exportation, respectively; the corresponding pressures were 30 Pa and -220 Pa. The air inlet is assumed to be at 25 °C. The calculated result is shown in Table 5. It can be seen that the second and third layers have different air flow, leading to large temperature non-uniformity. Because of the smaller flow, the majority of cells in the third layer had higher temperatures. The flow inconsistency was mainly attributed to the interference of air fans between the two layers.

Figure 9. CFD simulation model of the primitive pack.

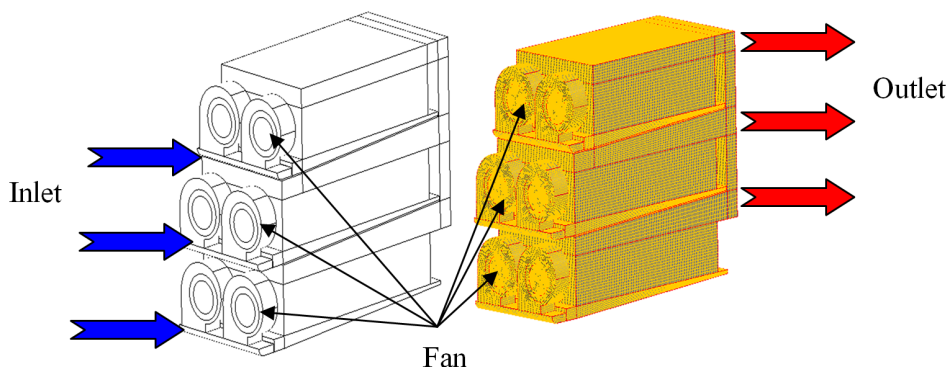


Table 5. Flow distribution results.

Layer No.	Flow/ Kg/s	Flow percent
1	0.0130	29.23%
2	0.0170	38.11%
3	0.0145	32.66%

Based on the flow distribution analysis, more in-depth CFD simulations for each layer were conducted. The simulation model of the third layer, for example, is shown in Figure 10. The section velocity contours of two fans are shown in Figure 11. It can be noticed that the middle area assumed larger air flow velocity in that the interference between the two fans existed. The cross-section velocity contour of the third battery layer is shown in Figure 12. It is obvious that flow non-uniformity existed among cells in the layer, causing the cell temperature gradient. Similar results can be obtained for the other two layers.

According to the analysis above, we can find that the undesired performance of the preliminary pack and cooling system design were due to the non-uniformity in the flow levels of battery layers. The design of the pack structure and the six air fans were unsatisfactory; the interference among fans had a considerably negative influence on cell temperature uniformity.

Figure 10. Simulation model of the third layer.

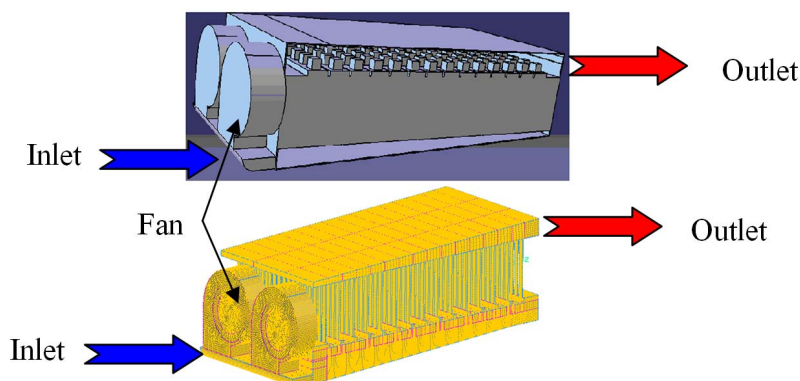
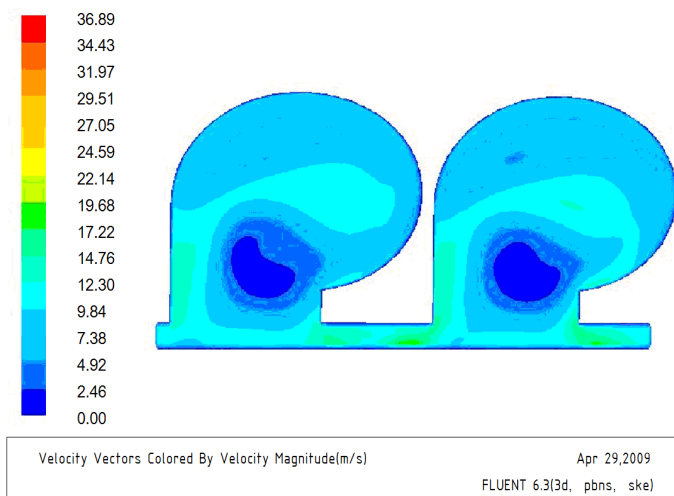
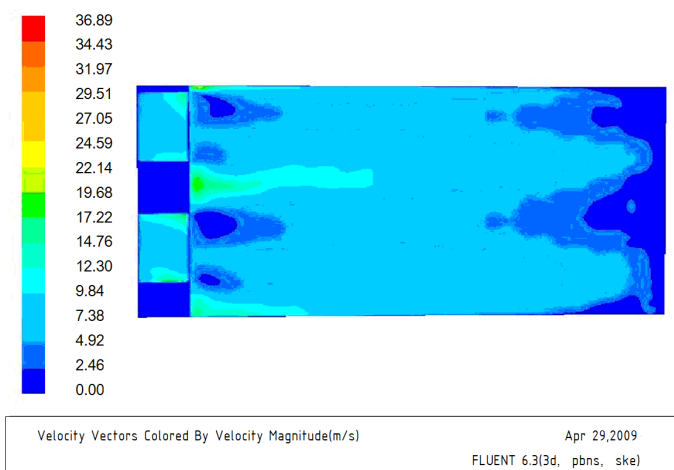


Figure 11. Section velocity contours of two fans.**Figure 12.** Cross-section velocity contour of the third layer.

4. Improved Thermal Energy Management

4.1. Enhanced Structure Design

In order to avoid the uneven flow distribution among layers which appeared in the original pack structure, 120 cells are placed in only one layer in the form of eight modules. Each module comprises 15 cells in series. Although the eight modules have a parallel topology, they are connected electrically in series. The configuration of the improved pack structure is shown in Figure 13. The primitive six air fans are replaced by one fan placed in the outlet to alleviate the flow non-uniformity among cells caused by the interference of multiple fans. The enhanced pack, together with its cooling system, is shown in Figure 14. The whole system consists of a box body (1), the battery pack (2) shown in Figure 13, an air intake duct (3), a DC/DC converter (4), an intelligent control unit (5), and a centrifugal fan (6). The pack dimensions and main electrical specifications are listed in Table 6. Please refer to our previous paper [28] to find more details on the structure design of the DC/DC converter and control unit for effectively dissipating the heat. The fan can provide larger air flow than those in the primitive design, with the maximum flow of 280 m³/h. The air enters the pack from the

intake duct under the suction role of the centrifugal fan, and then the convective heat transfer occurring at air ducts on the cell body and the internal gaps of the pack structure is able to cool the cells. After that, the air continues to dissipate the heat from the DC/DC converter and the controller and is finally extracted by the fan.

Figure 13. Improved battery pack structure.

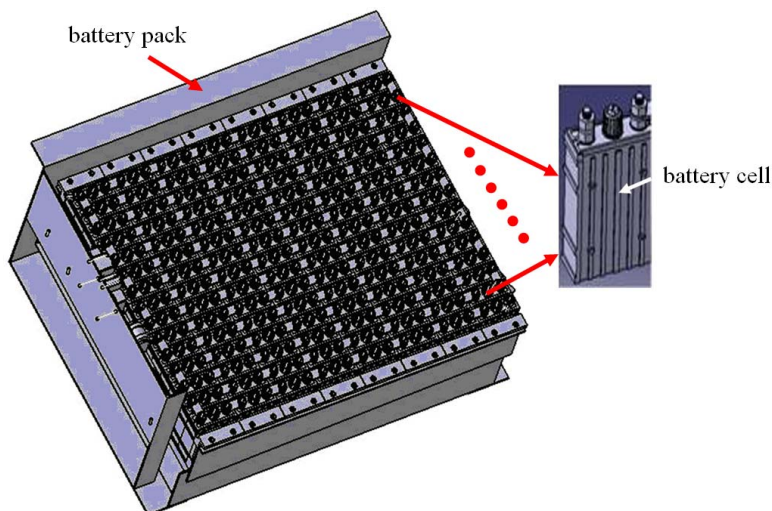


Figure 14. Configuration of the integrated pack and cooling system.

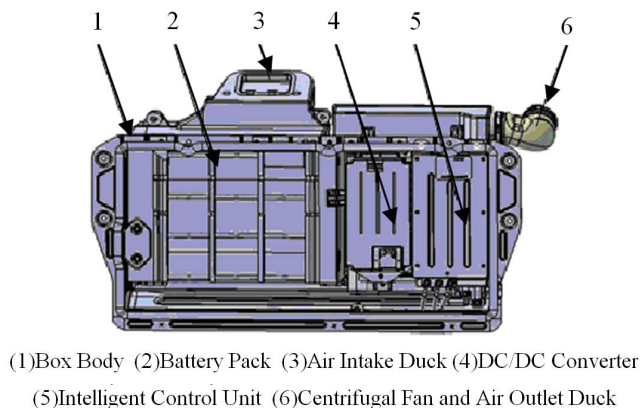


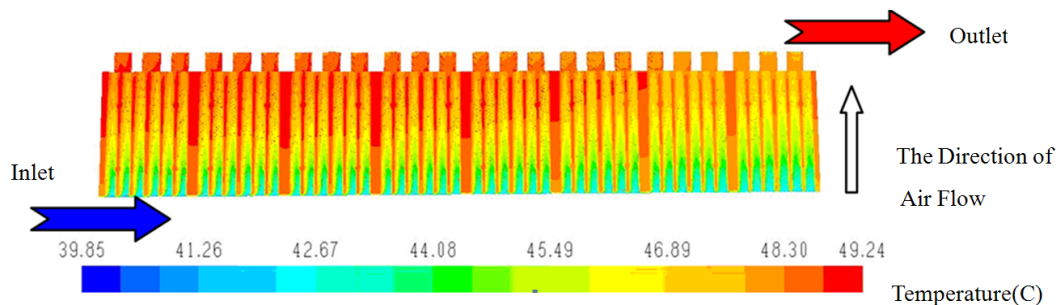
Table 6. Dimensions and main electrical specifications of the improved pack design.

Width	444 mm
Length	542 mm
Height	198 mm
Weight	35 kg
Nominal Capacity	6.5 Ah
Nominal Voltage	144 V
Number of cells	120

4.2. Simulation Validation

In the CFD simulation of the battery pack, the air flow at the inlet boundary provided by the fan was $140 \text{ m}^3/\text{h}$, and its temperature was assumed to be $35 \text{ }^\circ\text{C}$. Since the average heating power of the pack was measured to be 494 W in the practical HEV field test at $40 \text{ }^\circ\text{C}$, the heat flux of $718.5 \text{ W}/\text{m}^3$ was specified for the battery pack system in the simulation. Please refer to [27] for more details on the boundary conditions applied. The simulation result of the first row of cells is shown in Figure 15. We can see similar temperature change of air in the ducts and gaps for eight cells, indicating relatively uniform heat dissipation. The maximum temperature of cell surface is $49.3 \text{ }^\circ\text{C}$; the minimum is $45.5 \text{ }^\circ\text{C}$; the maximum deviation is therefore $3.8 \text{ }^\circ\text{C}$. It meets the performance index of thermal energy control depicted in Section 2. The simulation results of the other rows are similar.

Figure 15. Temperature field of the first row of cells in the enhanced pack design.



4.3. Experimental Validation

An experimental platform for evaluating the validity of the improved battery pack mainly was composed of an environmental chamber, a chassis dynamometer, a blower, and a data collection unit. The chamber was used to simulate the actual HEV environment parameters, such as ambient temperature, humidity, and sunlight intensity, such that the onboard test can be accomplished in a well-controlled indoor condition. The dynamometer was employed to load the HEV and control the vehicle speed to realize the specified driving cycles. In order to simulate the airflow around the vehicle during running, the blower was placed in front of the vehicle. The data collection system was to measure and record the cell temperature. The experiment arrangement is shown in Figure 16. The locations of temperature sensors (white circles) in the pack are shown in Figure 17. The sensors are numbered by using the indices of the matrix of 15 rows and 8 columns, for example, the number of the sensor in the fourth row and first column is 4-1.

To better evaluate the quality of thermal energy management of the pack, driving cycles inducing serious heating of energy storage device should be adopted. Two cycles simulating climbing (10% slope) and urban traffic jam were thus chosen. Please refer to [27] for the details of the two testing cycles. The results of assessing the temperature deviation among cells in the two tests are shown in Figure 18 and Figure 19. For good readability, we only show the temperatures from a part of sensors without loss of generality and validity. It can be found that the maximum temperature difference was $4.5 \text{ }^\circ\text{C}$ when the maximum cell temperature of $46.8 \text{ }^\circ\text{C}$ appeared in the climbing cycle; the maximum deviation was $5.2 \text{ }^\circ\text{C}$ when simulating the urban traffic jam. Therefore, the experimental

results demonstrate the validity of the improved battery pack thermal energy management design, according to the prescribed performance criterion in Section 2.

Figure 16. Experimental arrangement for performance assessment of the improved battery pack.

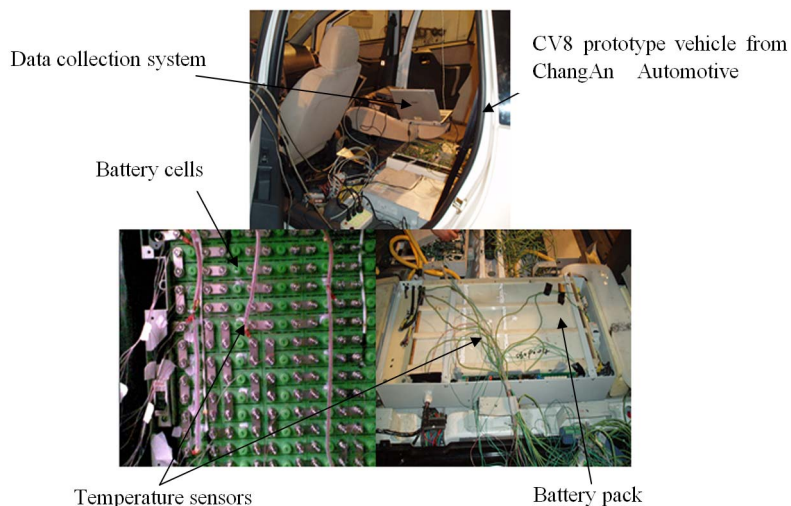


Figure 17. Sensor locations in the improved pack.

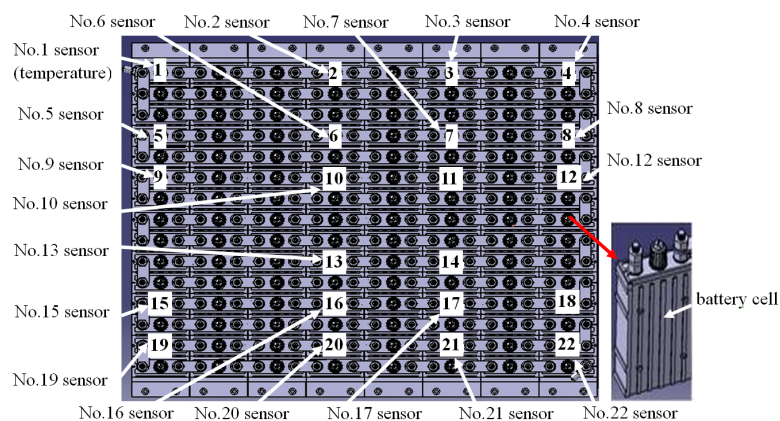


Figure 18. Temperature measurement in the climbing cycle.

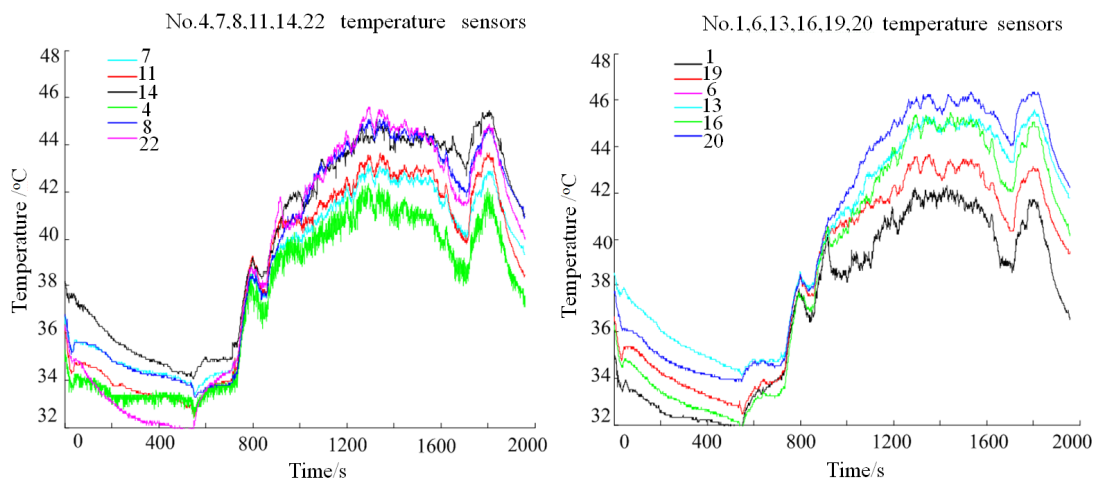
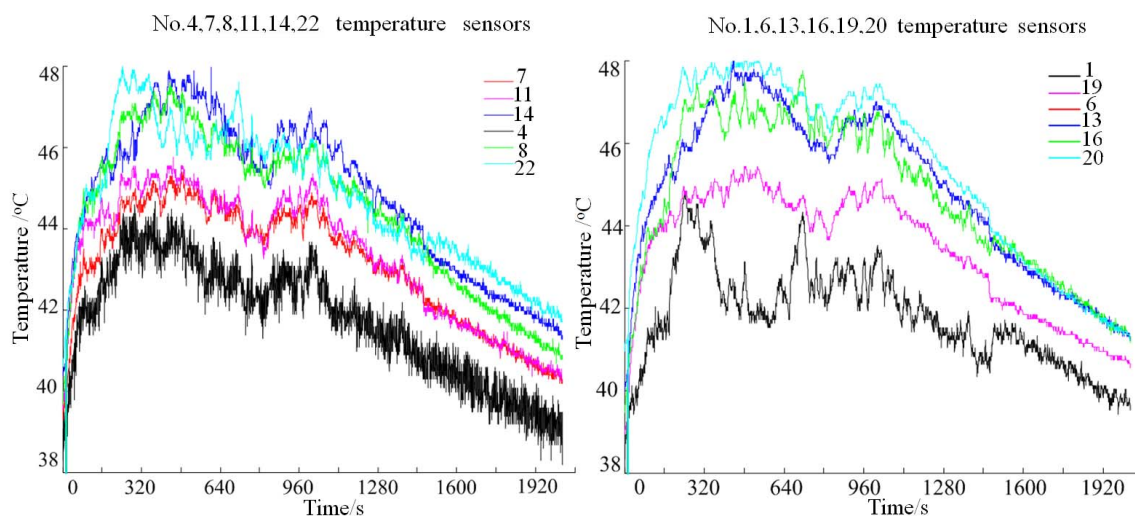


Figure 19. Temperature measurement in the urban traffic jam situation.

5. Conclusions

The impact of the temperature gradient on the cell lifetime consistency is first modeled for cells inside a HEV NiMH battery pack, based on Arrhenius equation, by analyzing the aging datasets collected under multiple environmental temperatures. This model, together with the requirement for the cell health consistency provided by the HEV manufacturer, is used as an evaluation criterion and guidance for the thermal energy management design of the NiMH battery pack adopted. It is found that the maximum temperature gradient should not be larger than 6 °C to guarantee the allowable cell life inconsistency. Since different types of cells typically have obviously dissimilar degradation characteristics, it is unreasonable to give a universal performance index for batteries of different chemistries or from different manufacturers, and a specific criterion is necessary for thermal energy management of the chosen battery to avoid under- or overdesign. According to the calibrated model, the applicability of a primitive NiMH battery pack design and its air cooling system without considering the actual relationship between the cell-health and temperature deviations is assessed, and its shortcomings are analyzed using computational fluid dynamics (CFD) analysis. The original three-layer structure is vulnerable to the uneven flow allocation among layers, and the large interference between two air fans in each layer also leads to serious flow non-uniformity among cells. In order to avert these deficiencies, an improved design scheme with one-layer pack structure and one potent cooling fan at the outlet is then proposed. The CFD simulation and experimental validation results show that the maximum temperature gradient among cells in the enhanced packaging and cooling design is less than 6 °C, verifying its effectiveness and superiority.

Acknowledgments

The authors would like to acknowledge Huei Peng at The University of Michigan (Ann Arbor, MI, USA) for insightful and constructive comments and language polishing. The research work was also partly supported by the National Natural Science Foundation of China (51075411) and Specialized Research Fund for State Key Laboratories in China (0301002109148).

References

1. Juul, N.; Meibom, P. Road transport and power system scenarios for Northern Europe in 2030. *Appl. Energy* **2012**, *92*, 573–582.
2. Williams, B.; Martin, E.; Lipman, T.; Kammen, D. Plug-in-hybrid vehicle use, energy consumption, and greenhouse emissions: An analysis of household vehicle placements in northern California. *Energies* **2011**, *4*, 435–457.
3. Ehsani, M.; Falahi, M.; Lotfifard, S. Vehicle to grid services: Potential and applications. *Energies* **2012**, *5*, 4076–4090.
4. Doucette, R.T.; McCulloch, M.D. Modeling the prospects of plug-in hybrid electric vehicles to reduce CO₂ emissions. *Appl. Energy* **2011**, *88*, 2315–2323.
5. Zou, Y.; Sun, F.; Hu, X.; Guzzella, L.; Peng, H. Combined optimal sizing and control for a hybrid tracked vehicle. *Energies* **2012**, *5*, 4697–4710.
6. Hu, X.; Sun, F.; Zou, Y. Estimation of state of charge of a lithium-ion battery pack for electric vehicles using an adaptive Luenberger observer. *Energies* **2010**, *3*, 1586–1603.
7. Xing, Y.; Ma, E.W.M.; Tsui, K.L.; Pecht, M. Battery management systems in electric and hybrid vehicles. *Energies* **2011**, *4*, 1840–1857.
8. Hu, X.; Li, S.; Peng, H. A comparative study of equivalent circuit models for Li-ion batteries. *J. Power Sources* **2012**, *198*, 359–367.
9. Hu, X.; Li, S.; Peng, H.; Sun, F. Robustness analysis of State-of-Charge estimation methods for two types of Li-ion batteries. *J. Power Sources* **2012**, *217*, 209–219.
10. Thomas, E.V.; Bloom, I.; Christophersen, J.P. Rate-based degradation modeling of lithium-ion cells. *J. Power Sources* **2012**, *206*, 378–382.
11. Rao, Z.; Wang, S.; Zhang, G. Simulation and experiment of thermal energy management with phase change material for ageing LiFePO₄ power battery. *Energy Convers. Manag.* **2011**, *52*, 3408–3414.
12. Duan, X.; Naterer, G.F. Heat transfer in phase change materials for thermal management of electric vehicle battery modules. *Int. J. Heat Mass Transf.* **2010**, *53*, 5176–5182.
13. Khateeb, S.A.; Farid, M.M.; Selman, J.R.; Al-Hallaj, S. Design and simulation of a lithium-ion battery with a phase change material thermal management system for an electric scooter. *J. Power Sources* **2004**, *128*, 292–307.
14. Khateeb, S.A.; Amiruddin, S.; Farid, M.M.; Selman, J.R.; Al-Hallaj, S. Thermal management of Li-ion battery with phase change material for electric scooters: experimental validation. *J. Power Sources* **2005**, *142*, 345–353.
15. Giuliano, M.R.; Prasad, A.K.; Advani, S.G. Experimental study of an air-cooled thermal management system for high capacity lithium-titanate batteries. *J. Power Sources* **2012**, *216*, 345–352.
16. Mahamud, R.; Park, C. Reciprocating air flow for Li-ion battery thermal management to improve temperature uniformity. *J. Power Sources* **2011**, *196*, 5685–5696.
17. Sabbah, R.; Kizilel, R.; Selman, J.R.; Al-Hallaj, S. Active (air-cooled) vs. passive (phase change material) thermal management of high power lithium-ion packs: Limitation of temperature rise and uniformity of temperature distribution. *J. Power Sources* **2008**, *182*, 630–638.

18. Rao, Z.; Wang, S.; Wu, M.; Lin, Z.; Li, F. Experimental investigation on thermal management of electric vehicle battery with heat pipe. *Energy Convers. Manag.* **2013**, *65*, 92–97.
19. Rao, Z.; Wang, S. A review of power battery thermal energy management. *Renew. Sustain. Energy Rev.* **2011**, *15*, 4554–4571.
20. Serrao, L.; Chehab, Z.; Guezenc, Y.G.; Rizzoni, G. An Aging Model of Ni-MH Batteries for Hybrid Electric Vehicles. In Proceedings of IEEE Vehicle Propulsion and Power, Chicago, IL, USA, 7–9 September 2005.
21. Laidler, K.J. *The World of Physical Chemistry*; Oxford University Press: Oxford, UK, 1993.
22. Laidler, K.J. *Chemical Kinetics*; 3rd ed.; Benjamin-Cummings: San Francisco, CA, USA, 1997.
23. Zhang, Y.; Wang, C.; Tang, X. Cycling degradation of an automotive LiFePO₄ lithium-ion battery. *J. Power Sources* **2011**, *196*, 1513–1520.
24. Zhou, C.; Qian, K.; Allan, M.; Zhou, W. Modeling of the cost of EV battery wear due to V2G application in power systems. *IEEE Trans. Energy Convers.* **2011**, *26*, 1041–1050.
25. Sarre, G.; Blanchard, P.; Broussely, M. Aging of lithium-ion batteries. *J. Power Sources* **2004**, *127*, 65–71.
26. Yang, H.; Piao, C. *Design Criteria of HEV Battery Module*; Technical Report for ChangAn Automobile Company Limited: Chongqing, China, 2007.
27. Chen, F. A Study on Temperature Uniformity of Ni-MH Batteries for Hybrid Electric Vehicle. Master's Thesis, Chongqing University, Chongqing, China, 2010.
28. Yang, Y.; Chen, F.; Qing, D.; Liang, C. Heat dissipation optimization of DC-DC and IPU for hybrid electric vehicle. *J. Chongqing Univ.* **2010**, *33*, 1–6.

© 2013 by the authors; licensee MDPI, Basel, Switzerland. This article is an open access article distributed under the terms and conditions of the Creative Commons Attribution license (<http://creativecommons.org/licenses/by/3.0/>).